1376. Crack detection in a pipe by adaptive subspace iteration algorithm and least square support vector regression

Youming Wang[1], Qing Wu[2]
[1, 2]School of Automation, Xi'an University of Posts and Telecommunications, Xi'an, 710121, China
[1]State Key Laboratory of Acoustics, Institute of Acoustics, Chinese Academy of Sciences, Beijing, 100190, China
[1]Corresponding author
E-mail: [1]*xautroland@163.com*, [2]*boyan315@163.com*
(Received 3 March 2014; received in revised form 20 April 2014; accepted 27 April 2014)

Abstract. A new combination method of beam-type finite element multiwavelet-based algorithm and least square support vector regression (LSSVR) algorithm is proposed for detecting the location and size of a crack in a pipe. According to operators of engineering problems, Rayleigh-Euler and Rayleigh-Timoshenko beam-type multiwavelets are constructed using the stable completion in the multiresolution finite element space. A rotational spring model is used for cracked pipe modeling and the local flexibility due to the crack is calculated by discrete approximation method. An adaptive subspace iteration algorithm (ASIA) is applied to efficiently approximate the exact solution of pipe model by adding new beam-type multiwavelets in each scale. To avoid the difficulty of constructing well-defined mathematical models, the normalized crack location and depth is detected by using LSSVR algorithm. The numerical and experimental results verify that the presented method can accurately identify the location and depth of crack in a pipe.

Keywords: pipe crack, multiwavelet, adaptive subspace iteration algorithm, least square support vector regression algorithm.

1. Introduction

Nowadays, pipes have been extensively applied in hydraulic engineering, petrochemical industry, agriculture engineering, civil engineering, etc. Research in vibration-based structural crack detection has been rapidly expanding over the recent several years [1-3]. Comparing with other non-destructive testing methods, i.e. ultrasonic, *X*-ray, magnetism method, the vibration-based methods are convenient and economical to determine the location and size of a crack from changes of vibration parameters, such as a reduction in the stiffness, increase in the damping, etc [4]. Much work has been dedicated to the crack modeling and associated crack diagnosis for vibration-based crack detection. The rotational spring model represents the crack as an additional rotational flexibility, which establishes the relationship between frequencies and crack information including location and size [5-9]. The bending moment model simulates the crack by comparing static bending moment and equivalent periodical bending moment [10]. The section modulus approach models the crack on the basis of appropriately reducing the section modulus of cracked structures [11-12]. In order to identify the location and depth of the cracks, a combined approach including model-based methed (forward problem) and crack search algorithm (inverse problem) becomes much emphasized by researchers [13-16]. Therefore, precise models of the structures with cracks and optimized crack algorithm are required for the forward problem. The cracked structures have usually been modeled to build the database of modal parameters using conventional finite element method (FEM) [13, 15], wavelet-based finite element method (WFEM) [17-18], etc.

Traditional wavelets are constructed by scaled and shifted versions of a single mother wavelet on a regularly spaced grid over a theoretically infinite or periodic domain. Therefore, they can not be constructed on finite meshes commonly encountered in finite element analysis.

Second-generation wavelets constructed by the lifting scheme [19-20] were developed to eliminate the restriction and deficiency of traditional wavelets and have gradually been applied in solving various mathematical and engineering problems. Castrillón-Candás and Amaratunga constructed spatially adaptive multiwavelets based on the lifting scheme to solve integral equations at high convergence rate [21]. Goh et al. constructed compactly supported biorthogonal multiwavelets with optimum time-frequency resolution [22]. Amaratunga et al. developed operator-customized wavelets based on stable completion and approximate Gram-Schmidt orthogonalization methods for finite element basis function of any given order on unstructured meshes of engineering problems [23-24]. Wang and Chen constructed a new kind of finite element multiwavelets based on the lifting scheme for adaptive structural modal analysis according to the operators of structural problems [25].

For the inverse problem analysis, it can be considered as the measurement of dynamic parameters and the search of crack location and depth from the crack detection database. The vibration data or signal of cracked structures is processed to detect the changes of modal parameters using signal processing method. The first three frequencies response functions of normalized crack location and depth are obtained by means of surface-fitting techniques [17, 26]. However, the difference between model-based solutions and measured frequencies will cause the failure of structural crack identification due to structural damping, boundary condition, etc. To solve this problem, the 'zero-setting' procedure was presented [27], which modified structural Young's modulus to coincide with the real structure work condition by using the measured uncracked natural frequencies. However, the modification of Young's modulus neglects many other factors, which may distort the modal parameters of a real structure.

In this paper, an adaptive subspace iteration algorithm (ASIA) is applied to solve the model of cracked pipe structures accurately. For the inverse problem analysis, we use the LSSVR algorithm [28-29] to search the optimized solution of pipe crack detection, which avoids the weakness of conventional model modification techniques. To investigate the robustness and accuracy of the proposed method, some numerical examples and experimental cases of cracked pipe are conducted.

2. The construction of beam-type finite element multiwavelets

The engineering eigenvalue problems are generally modeled by multiresolution finite element method. The multiresolution finite element space can be seen as a generalized hierarchical framework constructed from a wavelet perspective of finite element space. The scaling functions $\phi_{j,k}\ (k \in K(j))$ can be simply chosen to be the finite element interpolating functions and the wavelets $\varphi_{j,m}\ (m \in M(j))$ are the detail interpolating polynomials in the wavelet space [23-24], where $j \in J$ is the level of resolution, J is an integer index set associated with resolution levels, $K(j)$ is some index set associated with scaling functions of level j and $K(j) = K(j+1) \backslash K(j)$. To make the multiscale hierarchical matrix diagonally sparse, various finite element multiwavelets are constructed according to the operators of different problems.

2.1. Stable completion

The stable completion [30] is a method to construct interpolating multiwavelets with specific defined properties in the multiresolution finite element space. Comparing to the lifting scheme [19-20], the stable completion is more flexible and efficient to construct new multiwavelets with high vanishing moments, which is important for the scale decoupling of stiffness matrix and mass matrix in the multiscale computation. The stable completion assembles a new compact multiwavelet as a linear combination of several primitive wavelets and interior scaling functions:

$$\varphi_{j,m'} = \sum_m g_{j,m,m'} \varphi_{j,m} - \sum_k s_{j,k,m'} \phi_{j,k} = \sum_m g_{j,m,m'} \phi_{j+1,m} - \sum_k s_{j,k,m'} \phi_{j,k}\ , \quad (1)$$

where $g_{j,m,m'}$ and $s_{j,k,m}$ are the stable completion coefficients with $m' \in M(j)$. The stable completion provides us much freedom to design the wavelets by choosing appropriate stable completion coefficients. The stable completion coefficients can be computed by computing a basis for the null space of the local interaction matrix R_j in the scale-orthogonal relationship equations:

$$R_j \begin{bmatrix} s_{j,k,m'} \\ g_{j,m,m'} \end{bmatrix} = \begin{bmatrix} a(\phi_{j,k^*}, \phi_{j,k}) & a(\phi_{j,k^*}, \phi_{j+1,m}) \end{bmatrix} \begin{bmatrix} s_{j,k,m'} \\ g_{j,m,m'} \end{bmatrix} = 0, \tag{2}$$

where, ϕ_{j,k^*} are all the scaling functions on a given domain Ω_j, $\phi_{j,k}$ are the subset of scaling functions that are all interior in the domain Ω_j and $a(\bullet,\bullet)$ is the operator in the differential equations, engineering problems, etc. According to the scale-decoupling conditions in Eq. (2), we can get the principle of construction of the scale-decoupling wavelet bases according to the inheritance of vanishing moments property [23].

2.2. Rayleigh-Timoshenko beam-type multiwavelets

According to Rayleigh-Timoshenko beam theory, the equation of motion is of the form [31]:

$$\rho A \frac{\partial^2 w}{\partial t^2} - \frac{\partial}{\partial x}\left[GAK_s\left(\frac{\partial w}{\partial x} + \theta\right)\right] = 0, \tag{3}$$

$$\rho A \frac{\partial^2 w}{\partial t^2} - \frac{\partial}{\partial x}\left(EI\frac{\partial \theta}{\partial x}\right) + GAK_s\left(\frac{\partial w}{\partial x} + \theta\right) = 0, \tag{4}$$

where w denotes the transverse displacements, θ the rotation of cross-section, ρ the mass density per unit length, A the area of cross section, E the modulus, I the second moment of area, G the shear modulus, K_s is the shear correction factor. The operators corresponding to the stiffness matrix in the element free vibration have two types of multiwavelets in the form:

$$a_{11}(\varphi_i^1, \phi_j^1) = \int_0^1 GAK_s \frac{d\varphi_i^1}{dx}\frac{d\phi_j^1}{dx} dx, \tag{5}$$

$$a_{12}(\varphi_i^1, \phi_j^2) = \int_0^1 GAK_s \frac{d\varphi_i^1}{dx}\phi_j^2 dx = a_{21}(\varphi_i^2, \phi_j^1), \tag{6}$$

$$a_{22}(\varphi_i^2, \phi_j^2) = \int_0^1 EI\frac{d\varphi_i^2}{dx}\frac{d\phi_j^2}{dx} dx + l_e^2 \int_0^1 GAK_s \varphi_i^2 \phi_j^2 \, dx, \tag{7}$$

where $i \in J$. The operators for mass matrix are:

$$b_1(\varphi_i, \phi_j) = \int_0^1 \rho A \varphi_i \, \phi_j dx, \tag{8}$$

$$b_2(\varphi_i, \phi_j) = \int_0^1 \rho A \varphi_i \, \phi_j dx. \tag{9}$$

According to the operator of Rayleigh-Timoshenko beam problems, we can construct multiwavelets based on the stable completion method, which ensure the scaling functions and wavelet functions are orthogonal with respect to the operator (5)-(9). Figs. 1(a) and 1(b) show quadratic and cubic Rayleigh Timoshenko beam-type multiwavelets on the support (–1, 1), respectively.

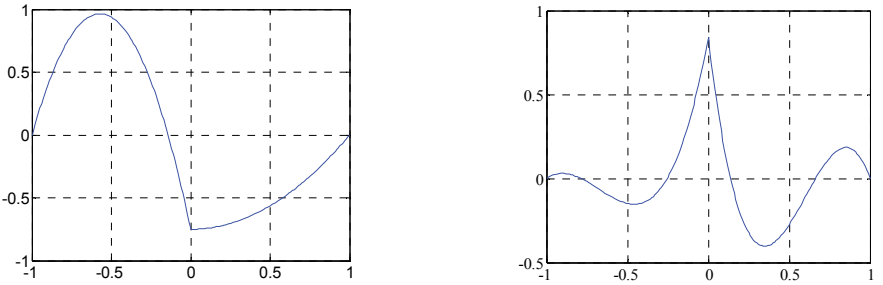

Fig. 1. Rayleigh Timoshenko beam-type multiwavelets: a) Quadratic, b) Cubic

2.3. Rayleigh-Euler beam-type multiwavelets

Considering rotary inertia of beam, the governing equation of transverse vibration of Rayleigh-Euler beam is (Reddy 2004 [31]):

$$\rho A\frac{\partial^2 w}{\partial t^2}-\rho I\frac{\partial^4 w}{\partial t^2\partial x^2}+\frac{\partial^2}{\partial x^2}\left(EI\frac{\partial^2 w}{\partial x^2}\right)=q(x,t), \tag{10}$$

where ρ, A, E and I have the same meaning as Rayleigh-Timoshenko beam. The operators for Rayleigh-Euler beam element can be derived as:

$$a\left(\varphi_i,\phi_j\right)=\int_0^1 EI\frac{d^2\varphi_i}{dx^2}\frac{d^2\phi_j}{dx^2}dx, \tag{11}$$

$$b\left(\varphi_i,\phi_j\right)=\int_0^1 \rho I\frac{d\varphi_i}{dx}\frac{d\phi_j}{dx}dx+l_e^2\int_0^1 \rho A\varphi_i\phi_j\,dx. \tag{12}$$

Fig. 2(a) shows a cubic Euler-Bernoulli beam multiwavelet with three vanishing moments on the support (0, 3). For quintic Hermite scaling functions, we can construct new multiwavelets on the support of two elements with two vanishing moments as shown in Fig. 2(b). To satisfy the operator-orthogonality in Eq. (12), new multiwavelets must be constructed with two more vanishing moments.

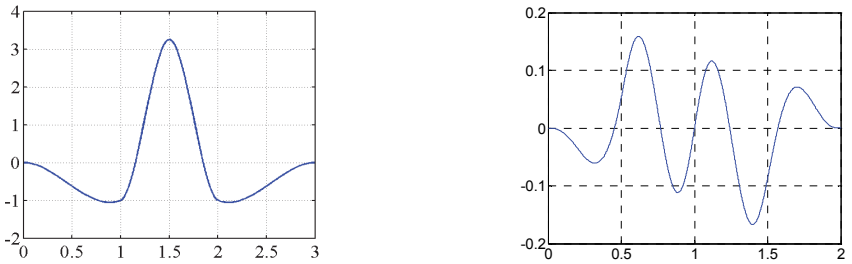

Fig. 2. Rayleigh Euler-Bernoulli beam-type multiwavelets: a) Cubic, b) Quintic

3. Crack detection based on ASIA and LSSVR

3.1. Pipe crack model

Fig. 3 shows a transverse crack of depth h is considered on a pipe and the crack section. The total length of the pipe is L_t, the lengths of pipe support are L_a and L_b. The inner and outer diameter of the pipe are D_a and D_b, resectively. The normalized crack location and depth are

$\beta = l/L$ and $\alpha = h/D_b$, resectively. The rotational spring model is used to model the cracked pipe. To overcome the difficulty in calculating local flexibility in the model, we consider a cracked pipe as a combination of a series of thin annuli. The stress intensity factor of a thin annulus can be calculated by analytical method presented by Tada et al. [32]. The stress intensity factor can be resolved to the desired accuracy when the number of divided thin annulus is large enough.

Considering the crack as a non-dimensional rotational linear spring [7-8], the cracked stiffness matrix can be written as:

$$K_c = \begin{bmatrix} (c_m)^{-1} & -(c_m)^{-1} \\ -(c_m)^{-1} & (c_m)^{-1} \end{bmatrix}, \tag{13}$$

where c_m is dimensionless compliance matrix calculated by local flexibility according to the strain energy theory in Reference [33]. The cracked stiffness submatrix K_c can be assembled into the global stiffness matrix and the cracked structural model based on the finite element multiwavelets is constructed. The solution of the eigenvalue problem for pipe structure can proceed as that of uncracked pipe structure.

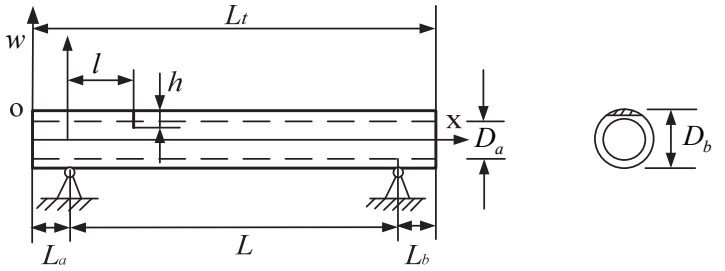

Fig. 3. Simply supported pipe with a crack

3.2. Adaptive subspace iteration algorithm (ASIA)

The eigenvalue equation for pipe structure:

$$K\lambda - \omega^2 M\lambda = 0, \tag{14}$$

can be discretized by interpolating multiwavelets at level j and the generalized eigenvalue problems can be obtained as:

$$K_{j+1}\lambda_{j+1} = \omega_{j+1}^2 M_{j+1}\lambda_{j+1}, \tag{15}$$

where K_{j+1} and M_{j+1} are multilevel stiffness and mass matrices at level $j+1$, λ_{j+1} and ω_{j+1} are the eigenvectors and eigenvalues at level $j+1$. The multilevel stiffness matrices K_{j+1} and M_{j+1} of eigenvalue equation can be denoted in the two-level form:

$$K_{j+1} = \begin{bmatrix} a(\phi_{j,p}, \phi_{j,q}) & a(\phi_{j,p}, \varphi_{j,q}) \\ a(\varphi_{j,p}, \phi_{j,q}) & a(\varphi_{j,p}, \varphi_{j,q}) \end{bmatrix}, \tag{16}$$

and:

$$M_{j+1} = \begin{bmatrix} b(\phi_{j,p}, \phi_{j,q}) & b(\phi_{j,p}, \varphi_{j,q}) \\ b(\varphi_{j,p}, \phi_{j,q}) & b(\varphi_{j,p}, \varphi_{j,q}) \end{bmatrix}. \tag{17}$$

Since the reference or exact solution may not be found in general engineering eigenvalue

problems, the eigenvalue solution at level $j+1$ is used to replace the exact eigenvalue solution and the error estimator is given:

$$\xi_j = \left|\frac{\omega_{j+1} - \omega_j}{\omega_{j+1}}\right|. \tag{18}$$

Given an initial domain Ω_j, an initial scale $j = 0$, a global tolerance ε and an iteration tolerance τ, an adaptive subspace iteration algorithm is presented to solve structural eigenvalue problems.

The multiscale method for eigenvalue problems is programmed as follows:

(1) Select initial vector X_j^0 at level j, let $Y_j = M_j X_j^0$. The initial eigenvector can be chosen randomly, but not orthogonal to λ_j, i.e. satisfy the equation $(X_j^0)^T M_j \lambda_j \neq 0$.

(2) Solve the equation $K_j X_j^1 = Y_j$. The scale-decoupling property of multilevel stiffness matrices ensures that it is unnecessary to factorize the stiffness matrices at each level.

(3) Construct new stiffness and mass matrices from:

$$\widetilde{K}_j = (X_j^1)^T Y_j, \tag{19}$$

and let $Y'_j = M_j X_j^1$, then:

$$\widetilde{M}_j = (X_j^1)^T Y'_j. \tag{20}$$

(4) Compute the approximate value of Λ_j^* from:

$$\widetilde{K}_j \lambda_j^* \Lambda_j^* = \widetilde{M}_j \lambda_j^*, \tag{21}$$

where:

$$\Lambda_j^* = \begin{bmatrix} \frac{1}{\omega_{j,1}^2} & & & \\ & \frac{1}{\omega_{j,2}^2} & & \\ & & \ddots & \\ & & & \frac{1}{\omega_{j,n}^2} \end{bmatrix}. \tag{22}$$

(5) Compute the iteration error estimator $\eta_{j,i}$ in the form:

$$\eta_{j,i} = \left|\frac{\Lambda_j^*(i+1) - \Lambda_j^*(i)}{\Lambda_j^*(i+1)}\right|, \tag{23}$$

and test whether it satisfies $\eta_{j,i} < \tau$. If it does not, go to step (6), otherwise, go to step (7).

(6) Regenerate $Y_j = Y'_j \lambda_j^*$., go to step (2).

(7) Let $\omega_j^* = (\Lambda_j^*)^{-1/2}$, compute the global tolerance ξ_j and test whether $\xi_j < \varepsilon$. If it does not, go to step (8), otherwise, go to step (9).

(8) Calculate the local error estimators $\delta_{j,n}$ in each local domains $\Omega_{j,n}$ in the following form:

$$\delta_{j,n} = \left|\frac{\omega_{j+1,n}^* - \omega_{j,n}^*}{\omega_{j+1,n}^*}\right|, \tag{24}$$

and let $\delta_j^{\max} = \max(\delta_{j,n})$. If $\delta_{j,n} \geq \theta\delta_j^{\max}$, the wavelet bases into the local domains and form new stiffness and mass matrices at the level j, go to step (1).

(9) Output the eigenvalue $\omega_j = \omega_j^*$ and the eigenvectors are computed in the form:

$$\lambda_j = X_{j,1}\lambda_j^*. \tag{25}$$

3.3. LSSVR algorithm

According to the structural risk minimization principle, the regression problems can be expressed as a constrained optimization problem in the form [28-29]:

$$\min J(\varpi, e) = \frac{1}{2}\varpi^T\varpi + \frac{C}{2}\sum_{i=1}^{l} e_i^2, \tag{26}$$

$$s.t.\ y_i = \varpi^T\Phi(x_i) + v + e_i,\ \ i = 1, \ldots, N, \tag{27}$$

where e_i is the error. The solution of LS-SVM regressor will be obtained after we construct the Lagrangian function:

$$L(\varpi, v, e, u) = J(\varpi, e) - \sum_{i=1}^{l} u_i\{\varpi^T\Phi(x_i) + v + e_i - y_i\}, \tag{28}$$

and a system of linear equations can be derived based on KKT condition:

$$\begin{bmatrix} 0 & 1_N^T \\ 1_N & \mho + \gamma^{-1}I_N \end{bmatrix}\begin{bmatrix} v \\ u \end{bmatrix} = \begin{bmatrix} 0 \\ P \end{bmatrix}, \tag{29}$$

where $P = [p_1, \cdots, p_N]^T$, $1_N = [1, \cdots, 1]^T$ and $u = [u_1, \cdots, u_N]^T$. Here, I_N is an $N \times N$ identity matrix, and $\mho \in \mathbb{R}^{N\times N}$ is the kernel matrix defined by:

$$\mho_{ij} = \Phi(x_i)^T\Phi(x_j) = \Xi(x_i, x_j). \tag{30}$$

The kernel function $\Xi(\bullet,\bullet)$ typically has several options, such as the linear, polynomial, radial basis function (RBF) kernel, etc. We choose the RBF as the kernel of LS-SVR.

3.4. Crack detection

According to linear fracture mechanics theory, the additional localized flexibility in crack vicinity can be represented by a lumped parameter element [16]. With the crack propagation, the local flexibility and dynamic characteristics of the pipe structure will change accordingly, which can be used to identify crack location and size. The determination of natural frequencies f for a given crack location and depth can be obtained by the inputs of normalized crack location β and depth α. The relationship between natural frequencies f_r, $r = 1, 2, 3, \ldots$ and crack parameter can be denoted as:

$$f_r = F_r(\beta, \alpha),\ \ r = 1, 2, 3, ..., \tag{31}$$

where F_r is the function relation. The identification inverse problem of pipe crack, determining the normalised crack location β and depth α, can be written as:

$$(\beta, \alpha) = F_r^{-1}(f_r),\ \ r = 1, 2, 3, ... \tag{32}$$

Usually, the crack location and size of the pipe structure can be identified by the first two frequencies. Because natural frequencies change a little when the crack appears at the node of corresponding order, the first three frequencies are always used as input parameters of inverse problem to identify structural crack.

The pipe crack can be accurately detected by the combination of multiwavelet-based element method and LSSVR algorithm. The identification process can be summarized as following.

(1) The cracked structure model was built using multiwavelet-based elements and the database of pipe structure employing first three natural frequencies of the pipe structure with different location and size are solved by ASIA.

(2) Construction of prediction model of pipe crack. The training sample set for the LSSVR model is built as $\{f_i \quad \alpha\}$, $\{f_i \quad \beta\}$ by use of the detection data and the regression parameter was solved by LSSVR algorithm.

(3) Extracting the first three frequencies of the pipe structure form vibration experiments based on FFT method.

(4) The first three measured natural frequencies are employed as input parameters and identifying the crack location and depth by the trained LSSVR.

4. Numerical and experimental results

4.1. Numerical investigation

To verify the validity of multiwavelet-based Rayleigh Euler and Rayleigh Timoshenko beam elements, a typical pipe with different length under different boundary condition are illustrated. The first three frequencies of uncracked and cracked pipe models are solved by ASIA. To predict the crack location and depth, multiwavelet-based cracked pipe models are used to detect the crack in a pipe under a given prediction error estimator.

Example 1. Given a simple supported pipe, the pipe geometries and the material properties are as follows: pipe length $L = 1$ m, $La = 0.005$ m, $Lb = 0.005$ m, inner diameter $D_a = 0.05$ m, outer diameter $D_b = 0.06$ m, Young's modulus $E = 1{\times}10^{11}$ N/m^2, $G = 6{\times}10^{10}$ N/m^2, material density $\rho = 7900$ kg/m^3, Poisson's ratio $\mu = 0.3$, shear correction coefficient $K_s = 5/6$.

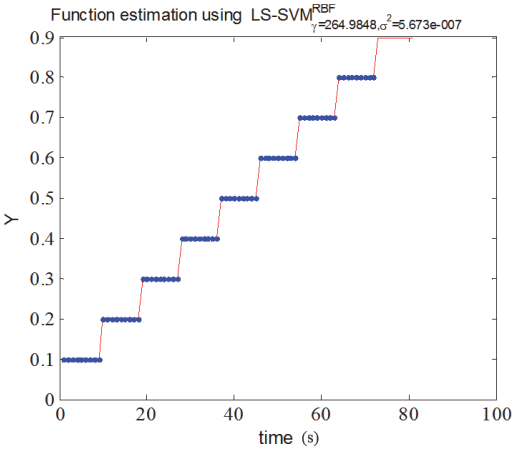

Fig. 4. LSSVM computation

The first three frequencies of the pipe crack model are obtained by using ASIA. Fig. 4 shows the LS-SVM results of the crack detection model in the region of the training points by using a Matlab/C toolbox for least squares support vector machines named LS-SVMlab [34]. In order to obtain an LS-SVM model (with the RBF kernel), two extra tuning parameters are given in Fig. 4,

where γ is the regularization parameter, determining the trade-off between the training error minimization and smoothness of the estimated function and σ^2 is the kernel function parameter. Let the error estimator of first three frequencies be 0.001 %, Table 1 illustrates the first three natural frequencies using ASIA and those of closed-form solutions in Reference [13] under various crack location and crack depth. It shows that the numerical solutions are in very good agreement with the closed-form solutions. Table 2 show the frequency error estimators in different spaces using quadratic Lagrange multiwavelets under $\beta = 0.5$ and $\alpha = 0.5$. Fig. 5 shows the error estimators of first three natural frequencies for the quadratic Lagrange multiwavelet solution. It can be seen that the solution of natural frequencies is convergent as the scale becomes larger and the convergence rate of the solution of first natural frequency is highest in that of three natural frequencies.

Table 1. Comparison of multiwavelet finite element and exact frequencies solution (the error estimator of frequency is 0.001 %)

β	α	Exact / rad/s			Multiwavelet solution / rad/s		
		ω_1	ω_2	ω_3	$\bar{\omega}_1$	$\bar{\omega}_2$	$\bar{\omega}_3$
0	0	248.39	980.09	2157.32	248.39	980.09	2157.32
0.10	0.15	248.22	978.18	2149.48	248.22	978.18	2149.48
0.10	0.45	241.24	883.71	1831.52	241.24	883.71	1831.52
0.20	0.20	246.54	960.66	2116.62	246.54	960.66	2116.62
0.20	0.40	230.41	834.35	1924.13	230.41	834.35	1924.13
0.30	0.50	200.28	807.08	2118.06	200.28	807.08	2118.06
0.30	0.35	225.61	879.70	2134.08	225.61	879.70	2134.08
0.40	0.25	236.44	962.73	2120.09	236.44	962.73	2120.09
0.40	0.50	188.96	906.57	2003.69	188.96	906.57	2003.69
0.50	0.30	226.23	980.07	1988.41	226.23	980.07	1988.41
0.60	0.25	236.42	963.23	2118.39	236.42	963.23	2118.39
0.60	0.45	198.64	918.65	2017.23	198.64	918.65	2017.23
0.70	0.30	233.07	908.35	2142.51	233.07	908.35	2142.51
0.80	0.50	218.53	771.63	1865.43	218.53	771.63	1865.43
0.80	0.20	246.41	960.53	2117.23	246.41	960.53	2117.23
0.90	0.30	245.86	944.76	2019.42	245.86	944.76	2019.42

Table 2. Error estimators of first three natural frequencies for the Quadratic Lagrange multiwavelet solution ($\beta = 0.5$; $\alpha = 0.5$)

Space	f_1 (Hz)	Error / %	f_2 (Hz)	Error / %	f_3 (Hz)	Error / %
V0 ($j = 0$)	202.57	16.53	1077.97	17.60	1823.61	17.46
V1 ($j = 1$)	191.77	10.31	1003.58	9.48	1705.56	9.85
V2 ($j = 2$)	179.91	3.49	959.83	4.71	1669.12	7.51
V3 (j =3)	176.31	1.42	941.18	2.67	1634.43	5.27
V4 ($j = 4$)	173.85	0.01	920.68	0.44	1585.69	2.13
V5 ($j = 5$)	173.84	0.00	918.02	0.15	1571.57	1.22
Exact solution	173.84	–	916.67	–	1552.56	–

To detect the crack in the pipe, the exact first three frequencies are used to be inputs of cracked pipe models based on the cubic Hermite multiwavelets shown in Fig. 2. Table 3 shows the prediction results of crack parameters based on the cubic Hermite multiwavelets while the error estimator of actual parameters is set to be 0.001 %. It can be concluded that the prediction results of crack parameters can efficiently approximate to high precision by ASIA. It can be found that the relative errors of the predicted normalized crack location and size are not more than 0.01 %.

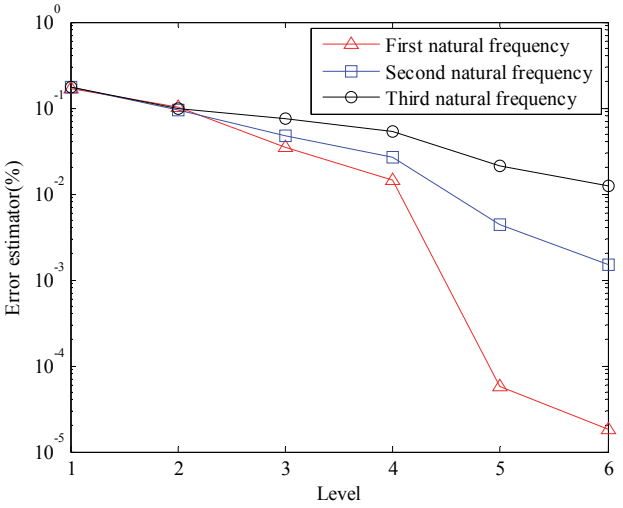

Fig. 5. Error estimators of first three natural frequencies for the quadratic Lagrange multiwavelet solution

Table 3. Comparison of predicted and actual crack parameters

Case	Actual β	Actual α	Exact / rad/s			Predicted β^* (%)	Predicted α^* (%)
			ω_1	ω_2	ω_3		
1	0.10	0.10	248.23	980.23	2157.45	0.1001(0.001)	0.0998(0.002)
2	0.10	0.50	239.18	858.90	1774.05	0.1001(0.001)	0.4994(0.0012)
3	0.20	0.20	246.54	960.66	2116.62	0.2000(0)	0.2000(0)
4	0.20	0.40	230.41	834.35	1924.13	0.2000(0)	0.3999(0.0003)
5	0.30	0.50	200.28	807.08	2118.06	0.2987(0.0043)	0.5003(0.0006)
6	0.30	0.30	233.16	907.77	2140.51	0.3011(0.0037)	0.2976(0.008)
7	0.40	0.20	243.49	972.61	2141.52	0.3999(0.0003)	0.1955(0.0225)
8	0.40	0.50	188.96	906.57	2003.69	0.4006(0.0015)	0.4989(0.0022)
9	0.50	0.30	226.23	980.07	1988.41	0.5000(0)	0.3000(0)
10	0.60	0.50	188.74	908.87	1996.27	0.6003(0.0005)	0.5012(0.0024)
11	0.60	0.40	208.72	929.20	2040.65	0.5996(0.0007)	0.3997(0.0008)
12	0.70	0.30	233.07	908.35	2142.51	0.7006(0.0009)	0.3001(0.0003)
13	0.80	0.50	218.53	771.63	1865.43	0.8003(0.0004)	0.5008(0.0016)
14	0.80	0.20	246.41	960.53	2117.23	0.7992(0.0010)	0.1989(0.0055)
15	0.90	0.50	238.90	855.43	1771.52	0.9005(0.0006)	0.5010(0.002)

4.2. Experiment investigation

In the vibration experiment of the cracked pipe, a Polytec Doppler laser vibrometer OFV-505/5000 and Sony EX system were used to measure the vibration of one point in the pipe. Force-hammer is used as current pulse exciting source. To reduce the reflection of the laser beam and spectral noise, retro-reflective tapes were put on the measurement point in the pipe. For each cracked pipe, the high-metrical frequencies can be obtained by using Fast Fourier transform (FFT) and spectrum zoom technique of Matlab R2010b. Figs. 6 and 7 show the experiment setup and cracked pipe, respectively. The pipe geometries and the material properties are as follows: $Lt = 1.450$ m, $La = 0.005$ m, $Lb = 0.005$ m, inner diameter $D_a = 0.05$ m, outer diameter $D_b = 0.06$ m, Young's modulus $E = 2.06\times10^{11}$ N/m^2, material density $\rho = 7390$ kg/m^3, Poisson's ratio $\mu = 0.3$. The crack of each pipe is generated by wire-cut machining with a molybdenum wire of diameter 0.18 mm.

Fig. 6. Experimental setup

Fig. 7. Cracked pipe

The quintic Hermite multiwavelets are used to construct the cracked pipe model, which is solved by ASIA. For the detection of pipe crack, the first three experimental measured frequencies are emplolyed as inputs of the prediction problems of pipe crack. For the prediction of crack location and depth, LSSVR algorithm is applied. For each cracked pipe, the high-metrical frequencies can be obtained by using the standard FFT program. A typical record including the impulse response signal and the power spectrum for $\beta = 0.480$ and $\alpha = 0.308$ is shown in Fig. 8. Table 4 shows the comparison of actual normalized crack parameters β and α and the predicted crack parameters β^* and α^*. For the given cases, the relative errors of β^* are not more than 5.31 % while the relative errors of α^* arrive at 11.82 %. Therefore, the proposed model-based crack detection method by the combination of multiwavelet-based elements and LSSVR algorithm is considered to be valid for actual application to detect fatigue cracks in a pipe.

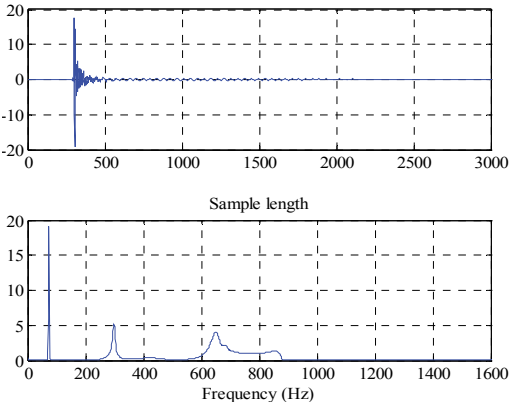

Fig. 8. FFT analysis on cracked pipe with $\beta = 0.480$ and $\alpha = 0.308$

Table 4. Identification results of cracked pipe

Case	Actual β	Actual α	Measured freqencies			Predicted β^* (Error / %)	Predicted α^* (Error / %)
			f_1 (Hz)	f_2 (Hz)	f_3 (Hz)		
1	0.245	0.108	78.01	311.22	697.09	0.253(3.27)	0.115(6.48)
2	0.245	0.133	76.97	308.98	686.83	0.232(5.31)	0.146(9.77)
3	0.341	0.177	76.76	309.26	676.96	0.329(3.52)	0.165(6.78)
4	0.393	0.203	76.54	307.33	663.77	0.377(4.07)	0.227(11.82)
5	0.480	0.308	73.50	295.07	656.67	0.459(4.37)	0.323(4.87)

5. Conclusions

A combination method of multiwavelet-based method and LSSVR algorithm is developed to detect the location and depth of crack in a pipe. Because of scale-decoupling property and efficient multilevel computation, the multiwavelet-based method is a useful tool to deal with high-precision

computation in structural crack identification. Based on the operators of structural problems, Rayleigh-Euler and Rayleigh-Timoshenko beam-type multiwavelets are constructed efficiently, respectively. An ASIA using multiwavelets is presented to efficiently approximate the exact solution of cracked pipe model. To identify the location and depth of a crack accurately, LSSVR algorithm is applied to eliminate the errors of frequencies between numerical simulation and experimental measurement. Numerical and experimental results verify that the proposed method can be utilized to detect crack location as well as crack size accurately. It is believed that the presented method can be extended to the high-precision detection of complex pipe structures with multiple cracks or filled with fluid.

Acknowledgements

The work in this article is supported by National Natural Science Foundation of China (No. 51205309, 51405387), Natural Science Basic Research Plan in Shaanxi Province of China (No. 2013JQ7025) and State Key Laboratory of Acoustics, Chinese Academy of Sciences (No. SKLA201309).

References

[1] **Doebling S. W., Farrar C. R., Prime M. B.** A summary review of vibration-based damage identification methods. Shock and Vibration Digest, Vol. 30, Issue 2, 1998, p. 91-105.

[2] **Bayissa W. L., Haritos N., Thelandersson S.** Vibration-based structural damage identification using wavelet transform. Mechanical Systems and Signal Processing, Vol. 22, Issue 5, 2008, p. 1194-1215.

[3] **Alvandi A., Cremona C.** Assessment of vibration-based damage identification techniques. Journal of Sound and Vibration, Vol. 292, Issue 1-2, 2006, p. 179-202.

[4] **Adams R. D., Walton D., Flitcroft J. E., Short D.** Vibration testing as a nondestructive test tool for composite materials. Composite Reliability, 1975, p. 159-175.

[5] **Dimarogonas A. D., Papadopoulos C. A.** Vibration of cracked shafts in bending. Journal of Sound and Vibration, Vol. 91, 1983, p. 583-593.

[6] **Papadopoulos C. A., Dimarogonas A. D.** Coupled longitudinal and bending vibrations of a rotating shaft with an open crack. Journal of Sound and Vibration, Vol. 117, Issue 1, 1987, p. 81-93.

[7] **Chaudhari T. D., Maiti S. K**. Modelling of transverse vibration of beam of linearly variable depth with edge crack. Engineering Fracture Mechanics, Vol. 63, Issue 4, 1999, p. 425-445.

[8] **Lele S. P., Maiti S. K.** Modelling of transverse vibration of short beams for crack detection and measurement of crack extension. Journal of Sound and Vibration, Vol. 257, Issue 3, 2002, p. 559-583.

[9] **Papadopoulos C. A.** The strain energy release approach for modeling cracks in rotors: a state of the art review. Mechanical Systems and Signal Processing, Vol. 22, 2008, p. 763-789.

[10] **Bachschmid N., Pennacchi P.** Identification of transverse crack position and depth in rotor systems. Meccanica, Vol. 35, 2000, p. 563-582.

[11] **Petroski H. J.** Simple static and dynamic models for the cracked elastic beam. International Journal of Fracture, Vol. 17, 1981, p. 71-76.

[12] **Christides S., Barr A. D. S.** One-dimensional theory of cracked Bernoulli-Euler beams. International Journal of Mechanical Science, Vol. 26, 1984, p. 639-648.

[13] **Nandwana B. P., Maiti S. K.** Detection of location and size of a crack in stepped cantilever beam based on measurement of natural frequencies. Journal of Sound and Vibration, Vol. 203, Issue 3, 1997, p. 435-446.

[14] **Naniwadekar M. R., Naik S. S., Maiti S. K.** On prediction of crack in different orientations in pipe using frequency based approach. Mechanical Systems and Signal Processing, Vol. 22, 2008, p. 693-708.

[15] **Sekhar A. S.** Crack identification in a rotor system: a model-based approach. Journal of Sound and Vibration, Vol. 270, 2004, p. 887-902.

[16] **Lee J.** Identification of multiple cracks in a beam using natural frequencies. Journal of Sound and Vibration, Vol. 320, Issue 3, 2009, p. 482-490.

[17] **Li B., Chen X. F., et al.** Detection of crack location and size in structures using wavelet finite element methods. Journal of Sound and Vibration, Vol. 285, 2005, p. 767-782.

[18] **Dong H. B., Chen X. F., et al.** Rotor crack detection based on high-precision modal parameter identification method and wavelet finite element model. Mechanical Systems and Signal Processing, Vol. 23, Issue 3, 2009, p. 869-883.
[19] **Sweldens W.** The lifting scheme: a construction of second generation wavelets. SIAM Journal of Mathematical Analysis, Vol. 29, Issue 2, 1997, p. 511-546.
[20] **Sweldens W.** The lifting scheme: a custom-design construction of biorthogonal wavelets. Applied and Computational Harmonic Analysis, Vol. 3, Issue 2, 1996, p. 186-200.
[21] **Castrillón-Candàs J., Amaratunga K.** Spatially adapted multiwavelets and sparse representation of integral equations on general geometries. SIAM Journal on Scientific Computing, Vol. 24, Issue 5, 2003, p. 1530-1566.
[22] **Goh S. S., Jiang Q. T., Xia T.** Construction of biorthogonal multiwavelets using the lifting scheme. Applied and Computational Harmonic Analysis, Vol. 9, Issue 3, 2000, p. 336-352.
[23] **D'Heedene S., Amaratunga K., Castrillón-Candás J.** Generalized hierarchical bases: a wavelet-Ritz-Galerkin framework for Lagrangian FEM. Engineering Computations, Vol. 22, Issue 1, 2005, p. 15-37.
[24] **Sudarshan R., Amaratunga K., Grätsch T.** A combined approach for goal-oriented error estimation and adaptivity using operator-customized finite element wavelets. International Journal for Numerical Methods in Engineering, Vol. 66, 2006, p. 1002-1035.
[25] **Wang Y. M., Chen X. F., He Z. J.** The construction of finite element multiwavelets for adaptive structural analysis. International Journal for Numerical Methods in Biomedical Engineering, Vol. 27, Issue 4, 2011, p. 562-584.
[26] **Xiang J. W., Zhong Y. T., Chen X. F., He Z. J.** Crack detection in a shaft by combination of wavelet-based elements and genetic algorithm. International Journal of Solids and Structures, Vol. 45, Issue 17, 2008, p. 4782-4795.
[27] **Adams R. D., Cawley P., Pye C. J., Stone B. J.** A vibration technique for non-destructively assessing the integrity of structures. Journal Mechanical Engineering Science, Vol. 20, Issue 2, 1978, p. 93-100.
[28] **Suykens J. A. K., Brabanter J., Lukas L., Vandewalle J.** Weighted least squares support vector machines: robustness and sparse approximation. Neurocomputing, Vol. 489, Issue 1-4, 2002, p. 85-105.
[29] **Suykens J. A. K., Gestel T., Brabanter J., Moor B., Vandewalle J.** Least Squares Support Vector Machines. World Scientific, Singapore, 2002.
[30] **Carnicer J. M., Dahmen W., Peña J. M.** Local Decomposition of refinable spaces and wavelets. Applied and Computational Harmonic Analysis, Vol. 3, Issue 2, 1996, p. 127-153.
[31] **Reddy J. N.** An introduction To the Finite Element Method. McGraw-Hill Science Engineering, Chicago, United States, 2004.
[32] **Tada H., Paris P. C., Irwin G. R.** The Stress Analysis of Cracks Handbook. ASME Press, New York, 2000.
[33] **He Y. M., Ye J. J., et al.** Discussion on calculation of the local flexibility due to the crack in a pipe. Mechanical Systems and Signal Processing, Vol. 23, 2009, p. 804-810.
[34] **Pelckmans K., Suykens J. A. K., Gestel T., Brabanter J., et al.** LS-SVMlab: a MATLAB/C toolbox for Least Squares Support Vector Machines. http://www.esat.kuleuven.ac.be/sista/lssvmlab.

Youming Wang received the MS and PhD degrees in Mechanical Engineering from Xi'an University of Technology and Xi'an Jiaotong University, Xi'an, China in 2006 and 2010, respectively. He is currently an associate professor at Xi'an University of Posts and Telecommunications. His current interests include fault diagnosis, structural crack identification and fatigue life analysis.

Qing Wu received the MS and PhD degrees in Applied Mathematics from Xidian University, Xi'an, China in 2005 and 2009, respectively. She is currently an associate professor at Xi'an University of Posts and Telecommunications, China. Her research interests include engineering optimization and pattern recognition.